Global magnetohydrodynamic simulation of reconnection and turbulence in the plasma sheet

Mostafa El-Alaoui,[1] Maha Ashour-Abdalla,[1,2] Robert L. Richard,[1] Melvyn L. Goldstein,[3] James M. Weygand,[1] and Raymond J. Walker[1,4]

Received 11 May 2010; revised 9 August 2010; accepted 23 August 2010; published 16 December 2010.

[1] Plasma sheet turbulence is examined by using a global MHD simulation. The simulation used idealized purely southward interplanetary magnetic field (IMF) driving conditions to eliminate the effect of solar wind and IMF variations. The results were compared with spacecraft observations of turbulence by computing power spectral densities and probability distribution functions. The fluctuations in the simulation were found to have properties characteristic of turbulence. The MHD simulation exhibited nested vortices on multiple scales, with the largest scales associated with reconnection outflows and the diversion of high-speed flows in the near-Earth region. The importance of strong localized reconnection regions in the simulation for driving the largest scale fluctuations supports the idea it is the main process driving turbulence in the plasma sheet. Interplay between turbulence and the reconnection process is probably present. Scaling arguments show that the scale at which turbulence is dissipated is consistent with the resistivity in the model.

Citation: El-Alaoui, M., M. Ashour-Abdalla, R. L. Richard, M. L. Goldstein, J. M. Weygand, and R. J. Walker (2010), Global magnetohydrodynamic simulation of reconnection and turbulence in the plasma sheet, *J. Geophys. Res.*, *115*, A12236, doi:10.1029/2010JA015653.

1. Introduction

[2] Recent studies [*Borovsky et al.*, 1997; *Borovsky and Funsten*, 2003; *Angelopoulos et al.*, 1999; *Chang*, 1999; *Klimas et al.*, 2000; *Weygand et al.*, 2007] have presented evidence that turbulence in the plasma sheet plays a major role in the physics of the magnetotail. Turbulent dissipation is known to be an effective mechanism for the heating of fluids and for the transfer of mass, momentum and energy [*Kolmogorov*, 1941; *Grant et al.*, 1962; *Kraichnan*, 1965]. Turbulence is characterized, in three dimensions, by a cascade of energy from (large) energy-containing scales, through an inertial range, down to dissipative scales as sketched from *Borovsky* [2004, Figure 5].

[3] It has long been recognized that the solar wind is turbulent [*Coleman*, 1968; *Roberts et al.*, 1987a, 1987b]. However, the techniques used for studying turbulence in the solar wind are generally not applicable to the magnetotail. In the solar wind, boundary effects are usually unimportant and the fluctuations generally constitute a random stationary time series [*Matthaeus and Goldstein*, 1982a; *Perri and Balogh*, 2010]. Because the solar wind flow is highly super-Alfvénic, one can assume the validity of the Taylor hypothesis [*Taylor*, 1938], under which one can interpret the time series of solar wind fluctuations in terms of wave numbers. If the Taylor hypothesis applies, there is a close relation between the temporal and spatial fluctuations. The Taylor hypothesis states that frequency ω is linearly related to the wave vector k (i.e., $\omega = \mathrm{k} \cdot \mathrm{v}$, where v is the plasma velocity) and is applicable if the structures within the magnetic field and flow evolve on a timescale longer than the time it takes them to pass the spacecraft. In the magnetotail, the flow rarely exceeds the Alfvén speed and thus time and spatial scales are inexorably intertwined. This has made it difficult to determine unambiguously the properties of magnetohydrodynamic (MHD) fluctuations in the magnetotail. It is even difficult to ascertain whether the fluctuations are, in fact, "turbulent." For instance, in the case of ideal gas dynamic turbulence the flow spectral density versus wave number generally has a slope of −5/3 on a logarithmic plot [*Kolmogorov*, 1941; *Grant et al.*, 1962], while for ideal isotropic incompressible MHD turbulence it has been predicted that the spectrum of power in magnetic fluctuations should fall off as −3/2 [*Kraichnan*, 1965] (although in the solar wind, that is rarely observed in magnetic field fluctuations and the spectral index is typically −5/3 [*Matthaeus et al.*, 1982; *Matthaeus and Goldstein*, 1982b]).

[4] Considerable observational evidence of turbulence in the plasma sheet has been found [*Consolini et al.*, 1996;

[1]Institute of Geophysics and Planetary Physics, University of California, Los Angeles, California, USA.
[2]Department of Physics and Astronomy, University of California, Los Angeles, California, USA.
[3]Laboratory for Geospace Science, NASA Goddard Space Flight Center, Greenbelt, Maryland, USA.
[4]Department of Earth and Space Sciences, University of California, Los Angeles, California, USA.

Copyright 2010 by the American Geophysical Union.
0148-0227/10/2010JA015653

Consolini and Michelis, 1998; *Borovsky et al.*, 1997; *Borovsky and Funsten*, 2003; *Lui*, 2001, 2002; *Weygand et al.*, 2005, 2006, 2007]. *Borovsky et al.* [1997] and *Borovsky and Funsten* [2003] examined the temporal fluctuations of the plasma sheet magnetic field and flow velocity. They employed a number of methods for identifying turbulence and found that the power spectral indices were in the range of −0.8 to −2.0 (flow) and −1.6 to −3.0 (magnetic field).

[5] These ranges are quite large and include both the *Kolmogorov* [1941] and *Kraichnan* [1965] values. To convert between frequency spectra and wave number spectra *Borovsky et al.* [1997] used a random-sweep model, which integrates the wave number spectrum over the velocity probability distribution function (PDF) and frequency. This model has theoretical and computational support, but its application to the plasma sheet has been criticized because conditions called for by the Taylor hypothesis are not present [*Tennekes*, 1975; *Chen and Kraichnan*, 1989]. However, *Weygand et al.* [2005] argued that power spectral indices do not unambiguously establish the presence of turbulence within the plasma sheet. They also considered the presence of intermittent turbulence, which results from spatial concentration of dissipation [*Biskamp*, 1993] by using PDFs. *Weygand et al.* [2005] examined the magnetic field spectral indices in a field aligned coordinate system and like *Borovsky et al.* [1997] found that the range of spectral indices was quite broad (average of −2.0 ± 0.4) for two of the field components. However, in the central plasma sheet, the transverse magnetic field component (approximately in the y direction) had a spectral index of −1.56 ± 0.04. This value is very close to the theoretical value of *Kraichnan* [1965]. *Weygand et al.* [2005] hypothesized that the other two components of the magnetic field, which have average spectral indices of −1.8 ± 0.2 and −2.3 ± 0.4, are affected by tail flapping, substorm dipolarizations, and surface waves while this azimuthal component is not so strongly affected. *Nykyri et al.* [2006a] have used data from the Cluster spacecraft in the cusp to construct magnetic field power spectra. They found slopes between −2.7 and −1 in the inertial range between –5 and –3 in the dissipative range.

[6] In the magnetosphere *Borovsky* [2004] suggested that large-scale shear flows at the magnetopause are a source for turbulence. Several researchers have constructed theoretical models of the plasma sheet with turbulence included [e.g., *Antonova*, 2000; *Antonova and Ovchinnikov*, 1999; *Borovsky et al.*, 1998]. The results suggest that eddy diffusion can fundamentally influence the plasma sheet configuration. *Borovsky et al.* [1998] obtained a diffusion time across the plasma sheet (z direction) of about 1 h. A number of local [*Nykyri and Otto*, 2001; *Nykyri et al.*, 2006b] and global MHD simulation studies have shown vortices forming at the magnetopause [e.g., *Walker et al.*, 1998, 2006; *Ashour-Abdalla et al.*, 1999, 2002; *White et al.*, 2001; *Slinker et al.*, 2003; *Hasegawa et al.*, 2004; *Fairfield et al.*, 2000; *Collado-Vega et al.*, 2007; *Claudepierre et al.*, 2008]. Vortices were found for both northward and southward IMF and have been interpreted as Kelvin-Helmholtz waves [*Walker et al.*, 1998; *Nykyri and Otto*, 2001; *Slinker et al.*, 2003; *Nykyri et al.*, 2006b; *Fairfield et al.*, 2007; *Collado-Vega et al.*, 2007; *Claudepierre et al.*, 2008]. Other simulations have reported vortices within the plasma sheet that were not associated with boundary oscillations [*El-Alaoui*, 2001; *White et al.*, 2001; *Ashour-Abdalla et al.*, 2002; *Walker et al.*, 2006; *El-Alaoui et al.*, 2009; *Ashour-Abdalla et al.*, 2009]. *Ashour-Abdalla et al.* [2002] and *Walker et al.* [2006] found large-scale vortices in the central plasma sheet during simulations of prolonged intervals with southward IMF.

[7] *Borovsky* [2004] has presented a detailed discussion of the problems in modeling MHD turbulence. The global MHD simulations that have produced large-scale vortices in the magnetosphere generally are too coarse to resolve turbulence even if it occurs. Studies of ordinary fluid turbulence indicate that ideally we need a code that resolves not only the large-scale geometry of the fluid flow but all scales down to the turbulence dissipation scale [*Pope*, 2000; *Matthieu and Scott*, 2000]. At the very least, an MHD global model should support the excitation and propagation of waves that have a relatively broad range of frequencies and wave numbers so that a turbulent cascade can be demonstrated before dissipation, whether numerical or physical, takes hold, or the limit imposed by grid resolution is reached.

[8] In this paper we use a global MHD simulation to address questions about the turbulence in the plasma sheet. First, we present an overview of the simulation results and show that a vigorous spectrum of fluctuations and eddies occur even under steady driving conditions. Next, we verify that the characteristics of the fluctuations observed in the simulation are consistent with observed magnetotail turbulence, mainly by considering the power spectral densities (PSDs) and PDFs of the fluctuations. We estimate the time scale at which dissipation dominates and show that is consistent with the PSDs. Our results indicate that spatial and temporally varying localized reconnection drives turbulence for steady southward IMF.

2. Simulation Model

[9] To help understand MHD turbulence in the magnetosphere we have carried out idealized global magnetospheric MHD simulations. The coupled magnetosphere-ionosphere, three-dimensional global MHD code we used for this study is based on a one-fluid description of the interaction between the solar wind and Earth's magnetosphere [*Raeder et al.*, 1995, 1998, 2001; *Frank et al.*, 1995; *El-Alaoui*, 2001; *El-Alaoui et al.*, 2004, 2008, 2009]. The numerical resistivity in the code is so low that an anomalous resistivity model must be introduced [*Raeder et al.*, 2001]. The ionospheric part of the model takes into account three sources of ionospheric conductance: solar EUV ionization, diffuse auroral precipitation modeled by assuming strong pitch angle scattering, and the accelerated electron precipitation associated with upward field-aligned currents. A detailed description of the MHD model is given by *Raeder et al.* [2001]. For the results presented in this paper a combination of low resistivity and small grid spacing was used to achieve a high magnetic Reynolds number that allowed turbulence to develop. Although the viscous interaction at the magnetospheric boundary in the MHD simulation is purely numerical, it yields an electric potential of about 30 kV, which is consistent with the observed value [e.g., *Sonnerup et al.*, 2001; *Reiff et al.*, 1981]. Both the resistivity model and the grid structure are discussed further

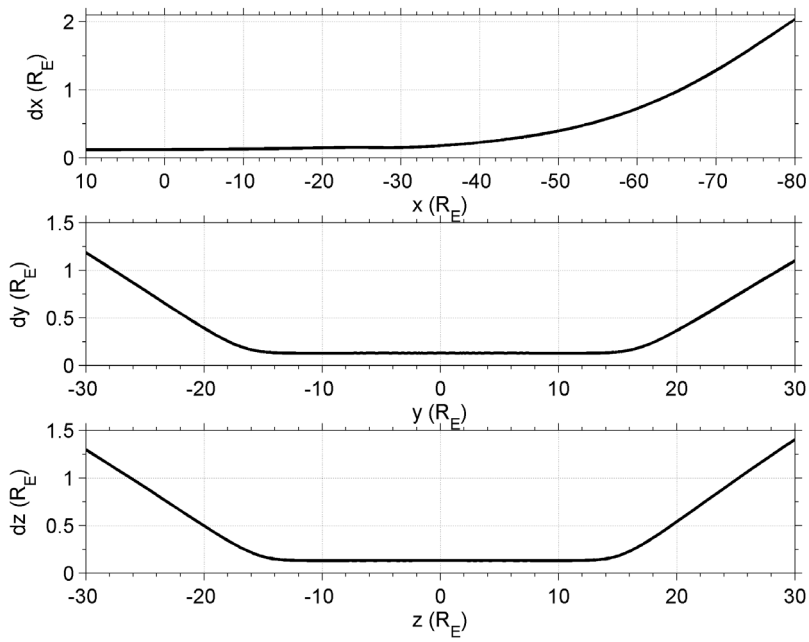

Figure 1. Distribution of the grid spacing in the MHD simulation. Shown are (top) the grid spacing in the x direction versus x, (middle) the grid spacing in the y direction, and (bottom) the grid spacing in the z direction.

below. We will discuss the contribution from reconnection in section 2.1.

2.1. Anomalous Resistivity

[10] Explicit resistivity is necessary in our code for reconnection to occur [*Raeder et al.*, 2001]. In the MHD simulation, the total electric field includes convective and resistive terms, and is given by: $\mathbf{E} = -\mathbf{v} \times \mathbf{B} + \eta\mathbf{J}$ is, where $\mathbf{v}$ is the bulk flow velocity, $\mathbf{B}$ is the magnetic field, $\mathbf{J}$ is the current density, and η is the resistivity. The resistivity η in our code is determined by applying the equations below.

$$\eta = \begin{cases} \alpha j_1^2 & \text{if } j_1 \geq \delta \\ 0 & \text{otherwise} \end{cases} \quad \text{where} \quad j_1 = \frac{|j|\Delta}{|B| + \varepsilon}$$

In this equation j is the local current density; B is the local magnetic field, Δ is the grid spacing and ε is a small number added to avoid dividing by zero. The coefficient α is determined empirically and is much less than 1. Similar models based on current-driven instabilities have been used successfully in local MHD simulations [*Sato and Hayashi*, 1979]. To avoid spurious dissipation there is a minimum current density threshold for resistivity controlled by the parameter δ (a value of 0.65 was used for these results) [*Raeder et al.*, 2001]. This threshold is calibrated such that explicit resistivity is switched on only at a very few grid points in intense current sheets. The effects of explicit and numerical resistivity in the simulation model are discussed by *Raeder et al.* [1996]. Further assessment of anomalous resistivity on substorm development is given by *Raeder et al.* [2001]. We set $\alpha = 0.05$, and the resulting maximum value for η was about 10^6 Ω·m.

2.2. Computational Mesh

[11] To study turbulence we need to resolve a wide range of scales from the large-scale geometry of the fluid flow down to the turbulence dissipation scale [*Pope*, 2000; *Mathieu and Scott*, 2000]. Present-day global MHD simulation codes have achieved a sufficient resolution, and thus sufficiently high magnetic Reynolds number, to allow us to investigate mesoscale MHD turbulence in the magnetosphere. High-resolution simulations of turbulence in the solar wind have demonstrated the feasibility of using finite difference codes to generate turbulent cascades with subsequent dissipation [e.g., *Goldstein et al.*, 1999].

[12] The MHD equations are solved on a Cartesian computational grid that is computed prior to the run by using three continuous functions, one for each simulation dimension, to distribute the grid points in the simulation system. We set the grid spacing to obtain high resolution in the central plasma sheet. The simulation used more than 52 million grid points: 540 in the x direction, 324 in the y direction and 300 in the z direction. The grid point spacing is shown in Figure 1. In the x direction the minimum grid spacing was 0.11 R_E (~700 km) and the maximum grid spacing was 3.84 R_E in the distant tail near a simulation outflow boundary. The grid spacing in the y direction had a minimum of 0.13 R_E (~828 km) and a maximum of 2.2 R_E. The grid spacing in the z direction had a minimum of 0.13 R_E (~828 km) and a maximum of 2.48 R_E. The regions of high-grid resolution were broad and encompassed the near Earth and midmagnetotail.

3. Simulation Setup

[13] We imposed a steady southward IMF with a magnitude of 5 nT at the upstream simulation boundary for more

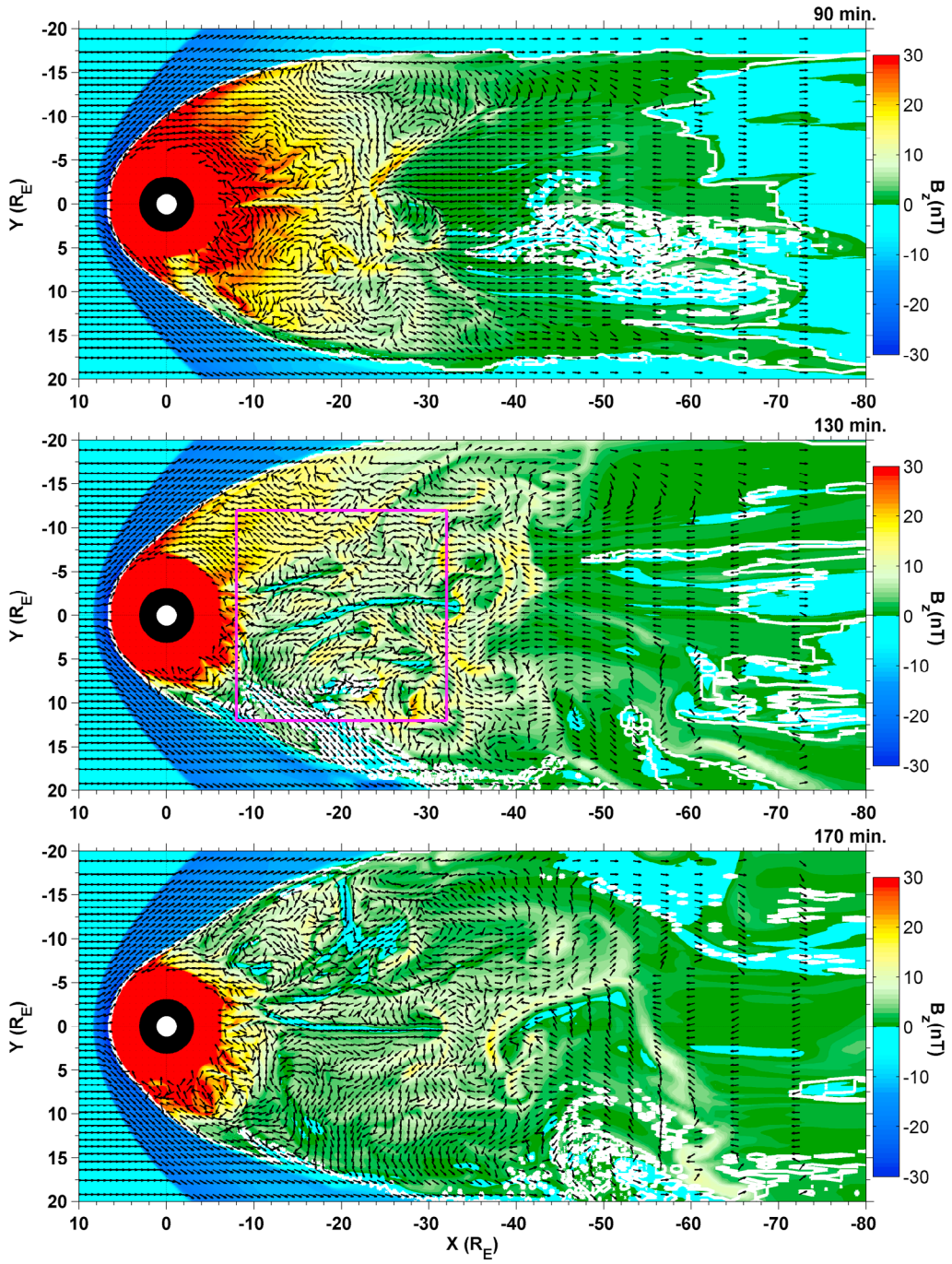

Figure 2. MHD solutions in the equatorial plane at three times: (top) 90 min after the start of the simulation, (middle) 130 min, and (bottom) 170 min. Superimposed are unit flow vectors in the equatorial plane and white solid lines showing the positions of the last closed field lines. The velocity vectors have been decimated by a factor of 6 in the x direction and by 6 in the in the y direction compared to the grid spacing.

than 3 h. The solar wind number density was 20 cm^{-3}, the thermal pressure was 20 pPa (temperature of 15.6 eV), and the velocity was 500 km/s in the x direction. The moderately high dynamic pressure confined the magnetotail to the high-grid resolution region. These conditions ensured that there was no turbulence in the solar wind and all fluctuations will be of internal origin. This experiment allowed us to investigate the turbulence driven by the magnetosphere's internal evolution. To obtain high-resolution time series of the simulation results for use in calculating power spectra and probability distribution functions we collected all MHD variables at all grid points in the equatorial plane every

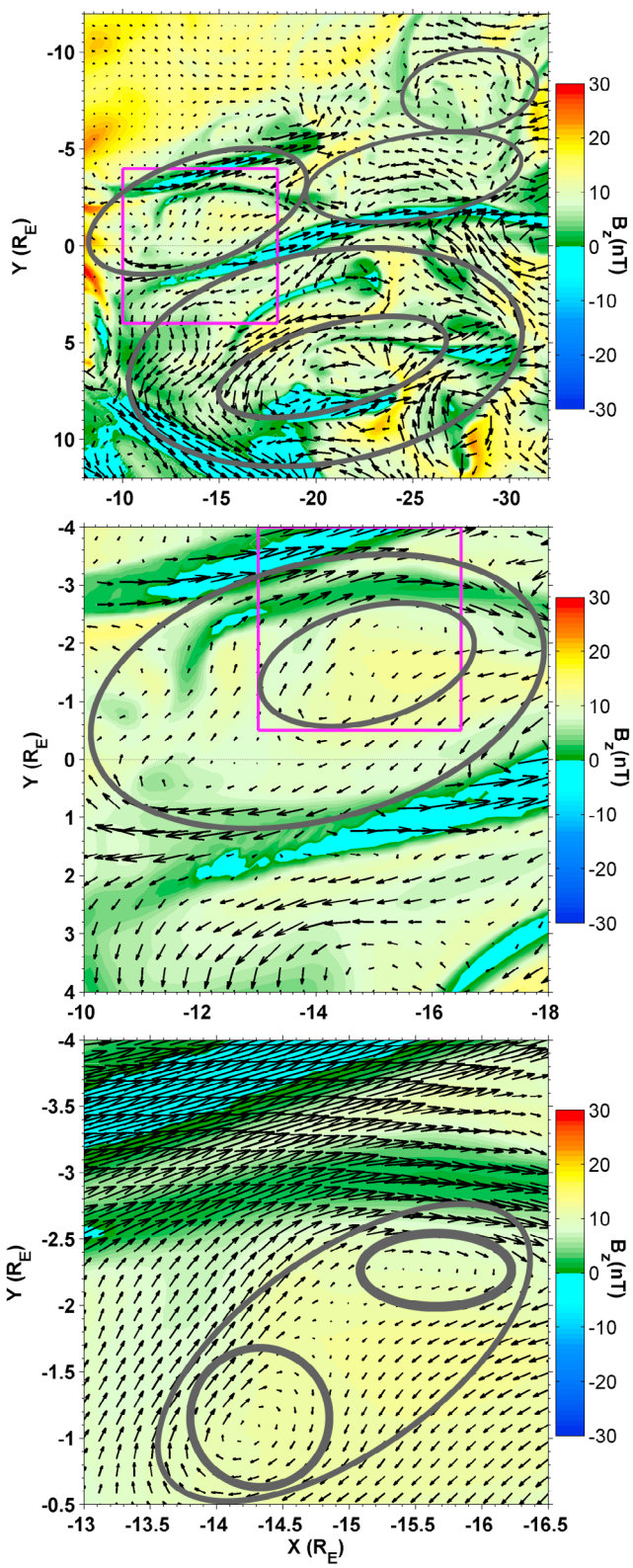

Figure 3. B_Z color contours and flow vectors at 130 min in the equatorial plane. The velocity vectors have been decimated (top) by a factor of 5 and (middle) by a factor of 3 in each direction. (bottom) All grid points are shown.

second. We then analyzed the results to determine the properties of the fluctuations generated in the simulation.

4. Simulation Results

[14] The simulation results showed magnetotail flows that were far from laminar. Snapshots taken at 90, 130, and 170 min into the run are shown in Figure 2. Three variables are superimposed in the equatorial plane at each time. The color contours display the B_Z component of the magnetic field, the black arrows show flows in the plane and the white isocontours give the locations of the last closed field lines. Even though the IMF was uniformly southward the tail neutral line was highly variable and the B_Z distribution shows numerous mesoscale structures. In particular, at 90 min, a highly irregular reconnection region existed between x = −30 and x = −60 R_E across the magnetotail. At 130 and 170 min much of the reconnection is localized, which we take to mean extending only part way across the tail. Localized reconnection can be identified as a region of intense flow reversal, from earthward to tailward, throughout the magnetotail coupled with reversals in the B_Z component of the magnetic field (white lines). Plots of the resistivity (not shown) reveal that the explicit resistivity was activated around the reconnection regions. The B_Z component evolved in a complex way during this interval and displayed filaments where it is large and positive at several locations. A spacecraft encountering this type of filament would experience magnetic field changes resembling dipolarization. Distinct vortices that have formed in the tail are apparent in Figure 2. High-speed flows that encounter the near-Earth region are deflected, forming vortices of various sizes in the magnetotail [*El-Alaoui*, 2001; *Ashour-Abdalla et al.*, 2002; *Walker et al.*, 2006; *El-Alaoui et al.*, 2009]. This region is characterized by a strong magnetic field, hot plasma at the inner edge of the plasma sheet, and strong coupling to the ionosphere. Nested within the largest vortices are smaller vortices. To illustrate the progressively smaller vortices seen in the plasma sheet we repeatedly magnify a region, seen in Figure 2 (magenta box) and Figure 3. Several vortices existed in this box, some of which are indicated by gray ovals (Figure 3, top). This panel also displays a magenta box within which one large and one small vortex are indicated. This region is further magnified in Figure 3 (middle) to reveal a yet smaller vortex nested in the larger vortex seen in Figure 3 (top). A magenta box encloses the small, nested vortex. This box is magnified in Figure 3 (bottom). Two still smaller vortices exist within the vortex from Figure 3 (middle). This pattern of nested vortices exists throughout the magnetotail during the simulation. The nested vortices in Figure 3 and the variations in B_Z in Figures 2 and 3 are both consistent with the presence of turbulence.

[15] To investigate the nature of the fluctuations in the magnetotail we calculated PSDs at different locations. Figure 4 shows the time histories and PSDs of the three magnetic field components over 3 h of the simulation at three points, all at z = 0 and x = −15 R_E with y: −5 R_E, 0 and 5 R_E. The time histories show numerous large amplitude fluctuations in all three components of the magnetic field, as well as in its magnitude (not shown). In the southward IMF case shown, time-varying localized reconnection is the most

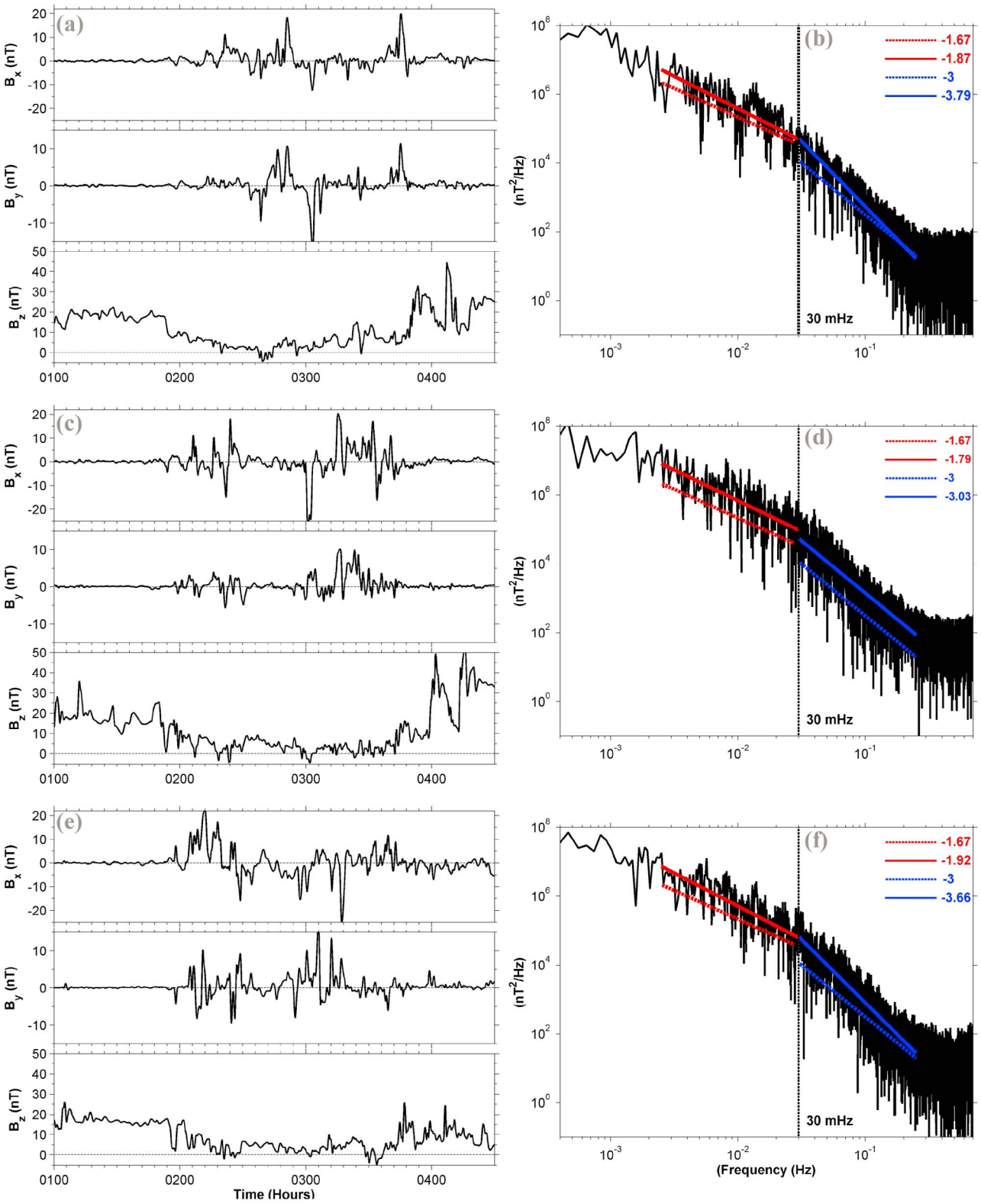

Figure 4. Time series and PSDs for the magnetic field. (left) Time histories of the three magnetic field components. (right) Power spectra for B_Z at three locations. All three locations are at x = −15 R_E and z = 0, with (a, b) y = −5 R_E, (c, d) y = 0, and (e, f) y = 5 R_E. The solid red (blue) lines are least squares fits at the inertial (dissipative) range.

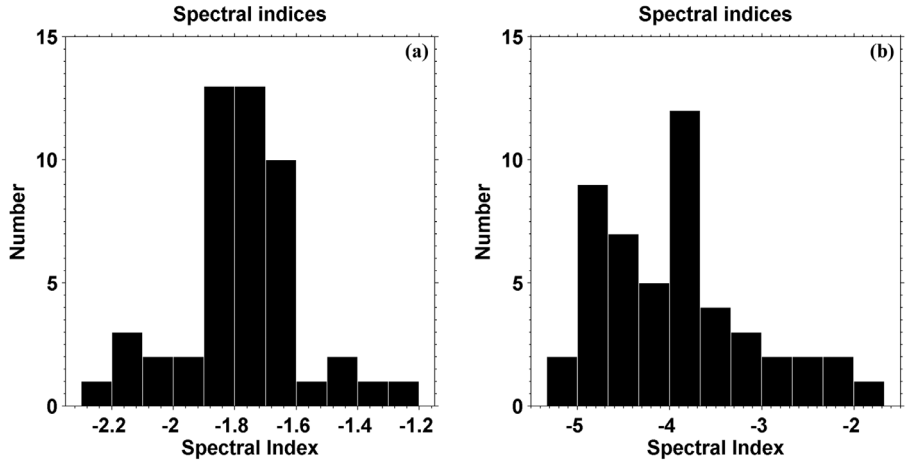

Figure 5. Distribution of spectral indices. Shown are histograms of the power spectral indices listed in Tables 1 and 2 for (a) the inertial range and (b) the dissipative range.

obvious source of the largest scale fluctuations [*El-Alaoui*, 2001; *Ashour-Abdalla et al.*, 1999, 2002; *Walker et al.*, 2006]. Theoretical analyses discussed in the introduction predict that in a turbulent state the PSDs will follow power law distributions in both the inertial range and in the dissipative range, with a greater slope in the latter. At each location the PSD includes a break in the slope consistent with a transition from the inertial to the dissipative range as well as a range at the lower frequencies without a well-defined slope consistent with the energy containing range. First, the three ranges were identified by eye, then least squares fits were performed for the inertial and dissipative ranges. The fluctuations in the PSDs are probably related to the sampling of the results every second versus the typical MHD time steps of 70 ms. The differences in slope among the three ranges are clear in the PSD plots (Figure 4). The predicted slope for the inertial range of −5/3 [*Kolmogorov*, 1941] is added for comparison. The observational situation is not clear for the dissipative range but values of −2.3 has been associated with whistler mode, Hall, or kinetic Alfvén wave turbulence [*Leamon et al.*, 1999; *Alexandrova et al.*, 2008] and a value of −4 has been associated with dissipation via electron Landau damping [*Sahraoui et al.*, 2009; *Alexandrova et al.*, 2009]. We show a line with a slope of −3 in the dissipative range, which is in the range seen in the solar wind (data available at http://arxiv.org/abs/1002.2539v1) and in the magnetosphere [*Nykyri et al.*, 2006a; *Vörös et al.*, 2005; *Matthaeus et al.*, 2008] for comparison. In the magnetotail plasma sheet the mechanisms that act to dissipate the turbulent fluctuations are not fully understood. The exact slope of the dissipative range may not be that important; as long as some reasonable dissipation exists at small scales the inertial range will be resolved. *Borovsky and Funsten* [2003] suggested several mechanisms that act to dissipate the turbulent fluctuations including coupling to the ionosphere, cyclotron resonance damping, Landau damping, reconnection, and plasma wave (anomalous) resistivity and viscosity.

[16] Table 1 lists the computed inertial range PSD slopes, and Table 2 lists the computed PSD dissipative range slopes at 49 locations in the equatorial magnetotail. The PSDs have slopes between −1.2 to −2.28 in the inertial range with a median value of −1.77 and a standard deviation of 0.21, which is less than the difference between the median value and −5/3. The breaks in the slope occur at around 30 mHz. In the dissipative range the slopes are between −2 to −5 with a median value of −3.9 and a standard deviation of 0.84. To further illustrate the PSD results we constructed histograms of the spectral slopes for the inertial ranges (Figure 5a) and for dissipative ranges (Figure 5b) at different locations. Figure 5a shows that a strong, narrow peak close to a spectral index of −1.77. This spectral index is close to Kolmogorov's result. *Weygand et al.* [2005] found that, based on observations, a peak in the distribution of slopes existed at a spectral index of −2.0 and a weak secondary peak at a slope of −1.6. Recall that, our calculations, unlike the observations, were for a quasi steady state under constant driving, and were sampled in a plane of symmetry. *Weygand et al.* suggested that neither Kolmogorov nor Kraichnan type turbulence were present and the plasma sheet magnetic field fluctuations were consistent with intermittent turbulence. Figure 5b shows that our distribution is broader with possibly a peak at a spectral index of −3.9. These results indicate that the fluctuations are consistent with theoretical turbulence [*Kolmogorov*, 1941].

[17] On average, the PSD slopes in the inertial range are lower (more negative) than −5/3, but are within a standard deviation at almost all values of x and y (Table 1). In the dissipative range, the spectral index is almost always between −2 and −5, with most values clustered between −3 and −5. These values are consistent with *Nykyri et al.* [2006a] bearing in mind that their measurements were in the cusp region. There is a trend toward more negative slopes for more tailward locations (Table 2). This suggests that the turbulent fluctuations in the inertial range spread out across the tail and the spectra become similar even though the dissipation increases tailward, toward the reconnection region. It is interesting that resistivity variations drive turbulence even though it is the major cause of dissipation. The dissipation performs two roles in plasma sheet turbulence in the simulation; on a large scale it leads to reconnection which drives turbulence and on small scales it dissipates energy. Although the dissipation was localized, the frequencies for the transition between the inertial and dissipative ranges at different locations were similar. All the

Table 1. Inertial Range[a]

	x						
y	−15	−10	−5	0	5	10	15
10.00	−1.90	−1.48	−2.07	−2.28	−2.18	−1.69	−1.21
15.00	−2.16	−1.82	−1.81	−1.75	−1.81	−1.71	−1.60
20.00	−1.87	−2.16	−1.90	−1.79	−1.97	−1.60	−1.88
25.00	−1.81	−1.95	−1.40	−1.72	−1.67	−2.01	−1.78
30.00	−1.76	−1.73	−1.65	−1.72	−1.72	−1.77	−1.70
35.00	−1.88	−1.61	−1.61	−1.78	−1.80	−1.63	−1.63
40.00	−1.50	−1.32	−1.83	−1.70	−1.85	−1.65	−1.85

[a]Power spectral indices at different locations in the magnetotail. Shown are the slopes of the power spectra, using a log-log scale, in the inertial range.

PSDs at these locations show three frequency ranges: the driving (energy containing) range, the inertial range, and the dissipative range.

[18] The nature of turbulence in a system is controlled by the ratio of the scale length for dissipation versus the scale length of the system that is quantified, for resistivity, by the magnetic Reynolds number. We calculated the magnetic Reynolds number that is the ratio of the magnetic diffusion time to the Alfvén transit time. It is given by $R_m = \mu_o LV/\eta$ where V is the Alfvén speed and L is the scale length of interest. A high Reynolds number means that the resistivity is dominant on a length scale much smaller than the scale length of interest. By using the typical resistivity produced in the simulation at locations where the current density exceeds the threshold for explicit resistivity the Reynolds number varied widely but was typically in the range 100 to 1000 for a typical plasma sheet scale length of 2 R_E. However, the values near the reconnection sites fell to less than 10. *Weygand et al.* [2007] used an extrapolation technique for the plasma sheet observations and found an effective magnetic Reynolds number to be between 7 and 110. These values are smaller than the above estimated Reynolds number. It is possible that the Reynolds numbers computed from the observations are controlled by the regions with the most dissipation. This idea is supported by our result that the transition frequency between the inertial and dissipation scales was very similar throughout the magnetotail. In contrast, *Vörös et al.* [2006], by estimating the dissipation scale [*Vörös et al.*, 2005] using plasma sheet flow data, found a value of 1600 which is comparable to our results.

5. Estimation of Dissipative Scale Using Mean Field Energy Equations

[19] In this section we consider what determines the frequency scale of the transition between the inertial and dissipative scale, and in the process, the spatial scale of this transition. To estimate the transition scale we start from the MHD energy equation. This equation can be written as follows:

$$\frac{\partial e}{\partial t} = -\nabla \cdot [(e+p)\mathbf{v}] + \mathbf{J}\cdot\mathbf{E}$$
$$\mathrm{e} = \frac{\rho \mathbf{v}^2}{2} + \frac{p}{\gamma - 1}. \tag{1}$$

In equation (1) ρ is the density,**v** is the flow velocity, p is the pressure, **E** is the electric field, **J** is the current density, e is the energy density, and γ is the ratio of specific heats (a value of 5/3 is used).

[20] Expanding (1) by using the explicit equation for the pressure we obtain

$$\frac{\partial}{\partial t}\left(\frac{\rho \mathbf{v}^2}{2}\right) = -\nabla\cdot\left[\frac{\rho\mathbf{v}^2}{2}\mathbf{v}\right] - (\mathbf{v}\cdot\nabla)p - \mathbf{J}\cdot(\mathbf{v}\times\mathbf{B}) + \eta\mathbf{J}^2, \tag{2}$$

where **B** is the magnetic field and η is the resistivity. To estimate the spatial scaling we assume a steady state $\frac{\partial}{\partial t} = 0$. Then (2) becomes

$$\eta\mathbf{J}^2 = \nabla\cdot\left[\frac{\rho\mathbf{v}^2}{2}\mathbf{v}\right] + (\mathbf{v}\cdot\nabla)p - \mathbf{J}\cdot(\mathbf{v}\times\mathbf{B}). \tag{3}$$

[21] We then replace variables with mean values and assume a typical scale length L to obtain the order of magnitude estimates we seek. We make substitutions (4) into (3)

$$\nabla \to \frac{1}{L};\ \mathbf{J} \to \frac{\overline{B}}{\mu_o L};\ \mathbf{v} \to \overline{v};\ p \to \overline{p}, \quad \text{and } \rho \to \overline{\rho}. \tag{4}$$

The result is given below.

$$L = \frac{\eta}{\mu_o \overline{v}} \frac{1}{1 + \frac{\overline{p}}{\overline{B}^2/\mu_o} + \frac{\overline{\rho}\overline{v}^2/2}{\overline{B}^2/\mu_0}}. \tag{5}$$

Simplify to obtain

$$L = \frac{\eta}{\mu_o \overline{v}} \frac{1}{1 + \frac{\overline{B}}{2} + \frac{M_A^2}{2}}, \tag{6}$$

where β is the plasma beta and M_A is the Alfvén Mach number.

[22] Assuming $\beta = 1$ on average and low flow speed the maximum scale length can then be given by

$$L = \frac{2\eta_{\max}}{3\mu_o \overline{v}}. \tag{7}$$

Now we apply this equation to the MHD simulation results. We choose an area in the equatorial plane from −25 R_E to −10 R_E in x direction and from −15 R_E to 15 R_E in the y

Table 2. Dissipative Range[a]

	x						
y	−15	−10	−5	0	5	10	15
10.00	−1.98	−3.73	−3.58	−2.13	−2.45	−3.97	−3.90
15.00	−2.03	−3.78	−3.76	−3.23	−3.83	−3.78	−3.16
20.00	−2.71	−2.39	−3.92	−4.48	−4.06	−3.54	−3.52
25.00	−2.83	−3.13	−3.93	−4.77	−4.78	−4.57	−3.34
30.00	−4.12	−4.28	−4.33	−4.30	−4.47	−4.44	−3.82
35.00	−4.99	−3.82	−4.86	−4.70	−5.31	−4.67	−3.82
40.00	−4.46	−4.83	−4.86	−5.20	−4.57	−4.91	−4.56

[a]Power spectral indices in the dissipative range at different locations in the magnetotail. Shown are the slopes of the power spectra, using a log-log scale.

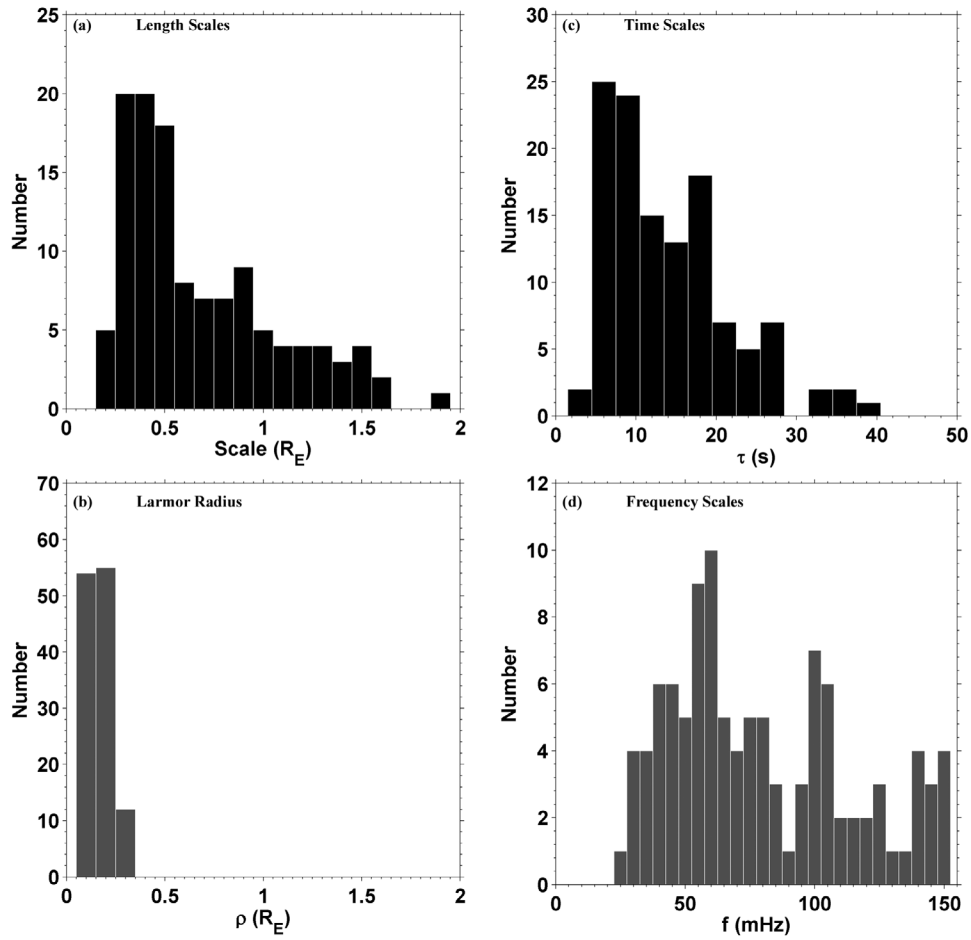

Figure 6. Scale length estimates. Shown are histograms of (a) the length scales, (b) the Larmor radii, (c) the time scales, and (d) frequencies.

direction to estimate the relevant values. For $\eta_{\max}$ in this equation we used the maximum value of η in this area, during each 2 min interval over the 3 h of southward IMF. The corresponding $\overline{v}$ values are the average speeds in the area during the same intervals. Figure 6a shows a histogram of the length scales given by equation (7) for the set of 2 min intervals. This panel shows that the scale extends from about 0.25 R_E to 1.6 R_E with most values in the range below 1 R_E and a median of 0.52 R_E. Although the Larmor radius plays no role in the MHD simulation we can estimate this quantity from the MHD parameters by using the average thermal speed, computed from the MHD density, pressure and magnetic field in the area defined above. The Larmor radius distribution is show in Figure 6b. All values of the Larmor radius were less than 0.3 R_E, which is lower than the scale lengths in the simulation shown in Figure 6a. Therefore the scales of the structures we are considering are larger than the Larmor radius, which is reasonable for an MHD simulation, as well as the MHD grid size. We also determined the time scale $\tau = \frac{L}{\overline{v}_A}$, where $\overline{v}_A$ is the average Alfvén speed with the result is shown in Figure 6c. The time scales that we found range from 5 s to 35 s. Finally we determined the frequency scale $f = \frac{1}{\tau}$ shown in Figure 6d. The frequency scale extends from 25 mHz to more than 120 mHz. Recalling that the PSDs showed breaks in the slope around 30 mHz (Figure 4), our frequency scale estimates are consistent with those results. Because fluctuations propagate rapidly through the magnetotail the transition scale is likely to represent a time and space average of dissipation controlled by the locations with maximum η. These regions are associated with reconnection which existed throughout the simulation run.

6. Probability Distribution Functions

[23] In this section our goal is to examine the Probability Distribution Functions (PDFs) from the MHD simulation and compare them to observations. *Weygand et al.* [2005, 2006] considered PDFs of fluctuations in the magnetic field for several different plasma sheet crossings recorded by Cluster using both the method applied by *Sorriso-Valvo et al.* [1999] in the solar wind and the two-point method developed by *Anselmet et al.* [1984]. PDFs of the observed fluctuations across different temporal and spatial separations are not Gaussian for small temporal separation, and the 4th moment of the PDFs (kurtosis) decreases nonlinearly with increasing temporal and spatial separation. The *Castaing et al.* [1990] fits show the same dependence on scale. *Castaing et al.* and *Sorriso-Valvo et al.* associate this nonlinear decrease to intermittent turbulence. Intermittency in magnetic turbulence can be inferred from a non-Gaussian

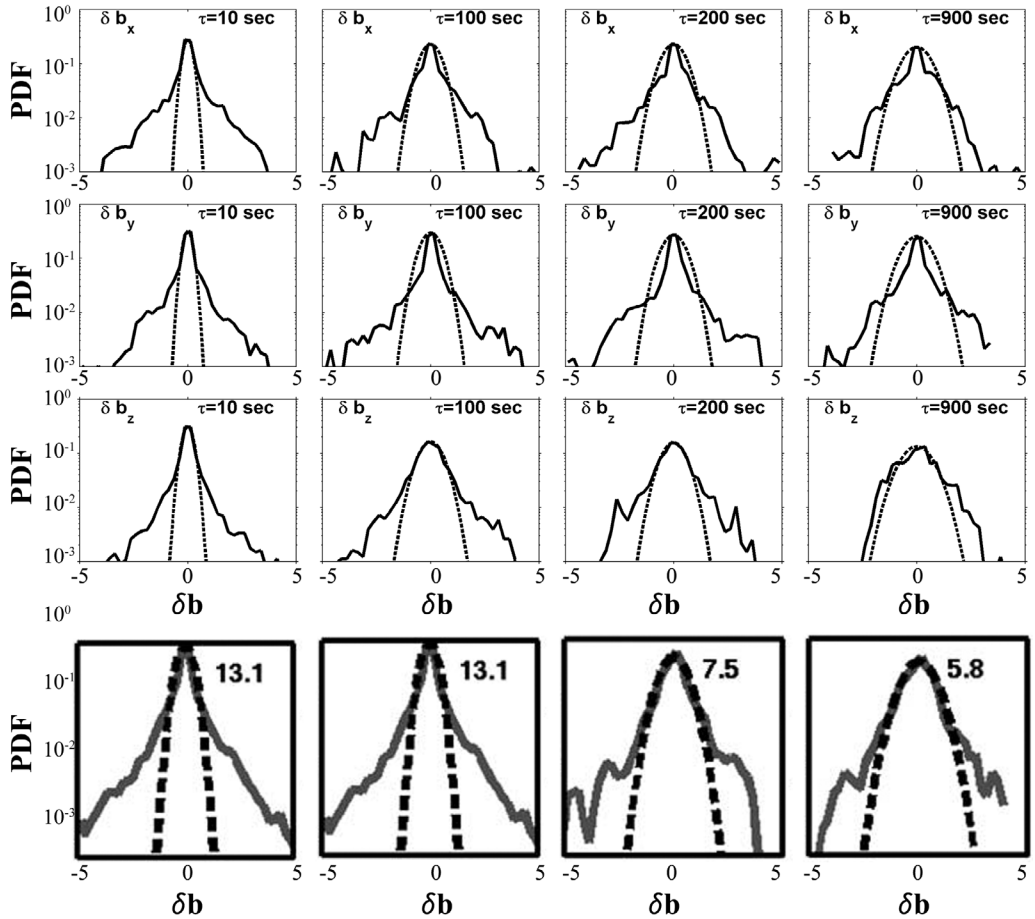

Figure 7. Probability distribution functions (PDFs) from MHD and the observations. The top three rows are from the three components of the magnetic field from simulation. The bottom row shows PDFs from B_X in the central plasma sheet from *Weygand et al.* [2005].

scaling of PDFs of the magnetic field fluctuations over time periods corresponding to frequencies that fall near the transition from the dissipation and inertial range. Our PDFs display this characteristic of intermittent turbulence. Intermittent turbulence corresponds to localization of dissipation [*Biskamp*, 1993], which is exactly what is observed in the distribution of resistivity in the simulation.

[24] We used the same technique as *Weygand et al.* [2005] to construct PDFs of the magnetic field fluctuations. We apply the function

$$\delta b_i = \frac{B_i(t+\tau) - B_i(t)}{\sqrt{\left\langle (B_i(t+\tau) - B_i(t))^2 \right\rangle}}, \tag{8}$$

where $B_i(t)$ is a component of the magnetic field at time t and $B_i(t + \tau)$ its value at a fixed time τ later [*Sorriso-Valvo et al.*, 1999]. First, a running average of 1000 s was removed from the magnetic field time series in order to eliminate longer period fluctuations in the magnetic field. As discussed by *Weygand et al.* [2005] the values of τ correspond to spatial lengths determined by the plasma speed. Small values of τ ($\tau \leq 10$ s) correspond to distances within the dissipative range for the simulation and large values of τ ($\tau \geq 900$ s) are associated with physical dimensions on the order of the driving scale of the plasma. Intermediate values of τ correspond to the inertial range. Figure 7 shows both results from the simulation and from *Weygand et al.* [2005]. The first three rows of Figure 7 show PDFs of the three components of the magnetic field in the simulation calculated by using (8) for four different values of τ. The dashed curves show Gaussian distributions for comparison that are fit by eye to the cores of the PDFs at x = −15 R_E and y = 5 R_E and z = 0 R_E. This distribution function illustrates how a measurement taken at a given time is correlated with a measurement taken at later times. If the relationship is random the result is a purely Gaussian distribution. All the PDFs show significant departures from a Gaussian distribution with large deviations from the average that can be described as "wings." For τ = 900 s the PDFs of the fluctuations in the magnetic field are the most similar to Gaussian distributions in particular for the B_X and the B_Z components of the magnetic field. In the last row we show PDFs of B_X from *Weygand et al.* [2005] for different values of τ from observations on August 15, 2001, in the central plasma sheet region. *Weygand et al.* [2005] consider τ = 10 s to correspond to the dissipative range, τ = 100 s and τ = 200 s to be in the inertial range, and τ = 900 s to be in the driving scale. The comparison between the simulation results and the observations show remarkable consistency, keeping in

mind that the simulation results are from a fixed plane of symmetry and at fixed position x = −15 R_E and y = 5 R_E.

7. Discussion and Conclusions

[25] High-resolution studies of turbulence in the solar wind have demonstrated the feasibility of using MHD finite difference codes to generate turbulent cascades and dissipation [e.g., *Goldstein and Roberts*, 1999]. Present-day global MHD simulation codes have achieved a sufficiently high resolution and magnetic Reynolds number to allow us to investigate MHD turbulence in the magnetosphere. To examine plasma sheet turbulence we used an MHD simulation of the magnetosphere. This simulation used idealized purely southward IMF conditions to eliminate the effect of solar wind and IMF variations. To compare the results with observationally based studies of turbulence we applied similar analyses to the simulation.

[26] We found that the fluctuations in the simulation had the characteristic properties of turbulence. We calculated PSDs and PDFs in the central plasma sheet and found not only that the results were consistent with observations but also that they had interesting physical implications. The MHD simulation exhibited nested vortices on multiple scales, with the largest scales associated with reconnection outflows and the diversion of high-speed flows in the near-Earth region.

[27] We calculated PDFs at different locations in the plasma sheet and we found that for smaller time scales the distribution is not Gaussian, revealing nonrandom correlations in the fluctuations. The observations showed similar patterns to those by *Weygand et al.* [2005]. The PSDs from the simulation showed all three frequency ranges expected from theoretical considerations: the driving or energy containing range, the inertial range and the dissipative range, with clear breaks between the different ranges. The PDFs and the localization of dissipation support the conclusion that the turbulence is intermittent in the simulation.

[28] In the inertial range we found the PSD slopes were clustered around an average value of −1.77. Both *Weygand et al.* [2005] and *Borovsky et al.* [1997] and *Borovsky and Funsten* [2003] found somewhat steeper slopes: [*Weygand et al.*, 2005] found PSD slopes near −2.0 and *Borovsky et al.* [1997] found PSD slopes in the range of −1.6 to −3.0. Bearing in mind that our calculations, unlike the observations, were for a quasi steady state under constant driving, and were sampled in a plane of symmetry, the agreement is very good. Our average value is within the ranges found based on observations. While the observed ranges were quite large and included both the *Kolmogorov* [1941] and *Kraichnan* [1965] spectral indices, the median value of the simulation results is close to Kolmogorov's result. This may be because the simulation is for idealized driving conditions and the results were sampled in a plane of symmetry, ensuring that the simulation results are all from the central plasma sheet.

[29] The dissipation included in the MHD simulation resulted in realistic values for the transition between inertial and dissipative scales, which was also consistent with an order of magnitude estimate based on mean values of MHD parameters in the plasma sheet. In the dissipative ranges we found a broader distribution with an average spectral index of −3.9. To our knowledge, this number is not as well constrained in the observations or the theory in the plasma sheet. It is remarkable that the transition between the inertial range and the dissipative range is consistently near 30 mHz at all locations considered, even though the major dissipation in the simulation, the anomalous resistivity, varies over orders of magnitude in space and time.

[30] In spite of variations in dissipation, PSD slopes at different locations are consistent, suggesting that energy transport is smoothing out the variations. This is similar to a pot of water being heated on an uneven open flame. The entire liquid will be at the boiling point because heat is being transported efficiently. A further factor to be considered is the influence of the ionosphere, which could add to dissipation or could intensify variations owing to the dependence of ionospheric conductivity on field-aligned currents. Correctly resolving the turbulent cascade may be accounted for in part by recent improvements in the accuracy of MHD simulations [e.g., *Guild et al.*, 2008; *El-Alaoui et al.*, 2009]. The success in simulating turbulence gives us confidence that MHD can be used to further investigate turbulence under both idealized and realistic conditions. The fine details of the dissipation do not seem to significantly affect the overall turbulent spectrum, which we show has realistic properties. In this view, correctly reproducing a spectrum of eddies in the simulation, which leads to realistic transport, is more important than the detailed dissipation model.

[31] There are several possible sources of plasma sheet turbulence. One is the external source of solar wind variations and turbulence. Turbulence in the solar wind has been extensively studied [e.g., *Bruno and Carbone*, 2005]. On the other hand several internal possibilities exist. These include shear flow instabilities, MHD instabilities in the inner magnetosphere (e.g., interchange or ballooning modes). Another possibility is that the turbulent flow field is feeding back on the reconnection process that will put the plasma sheet into self sustaining turbulent state [*Matthaeus and Lamkin*, 1986]. Variations in ionospheric conductivity may also lead to turbulence [*Walker et al.*, 2006; *El-Alaoui et al.*, 2009]. Another source of turbulence is the rapid variations associated with localized reconnection. The existence of strong localized reconnection regions with high-speed outflows in our results supports the idea that this is the main process driving turbulence in the plasma sheet. Dissipation in general should decrease fluctuations, but if the dissipation is localized it can drive flows in part of the plasma sheet that start the turbulent cascade. When a high-speed reconnection outflow reaches the near-Earth region it is diverted leading to a large, that is several R_E across but smaller than the width of the magnetotail, vortices in the driving scale. The existence of a strong spectrum of turbulent eddies may feedback on the reconnection process as well, leading to a very complex interplay between turbulence and dissipation.

[32] An interesting feature of the plasma sheet is that dissipation, which is normally thought of as a sink for the energy contained in the turbulent fluctuations, is also a catalyst of large-scale flows through the magnetic reconnection process that is very active during southward IMF conditions. In the simulation, local current sheet thinning concentrates dissipation in local regions leading to frequent localized reconnection events, consistent with observations.

The existence of a turbulent spectrum in the simulation may contribute to the patchiness of the reconnection in a feedback loop. It is not straightforward to suppress the feedback mechanism because fluctuations are present in most or all of the MHD simulations using this model [e.g., *Guild et al.*, 2008] though detailed analyses were not performed. We have not observed a "quiet" fluctuation-free state for southward IMF. We note, however, that even if magnetotail reconnection begins on a large scale; that is, extending across the whole magnetotail, the resulting fast flows will break up into large vortices in the near-Earth region which can initiate turbulence. Therefore this simulation indicates that the overall state of the plasma sheet under steady southward IMF and laminar solar wind flow is turbulent, which can strongly influence transport and dissipation in the region.

[33] **Acknowledgments.** Research at UCLA was supported by NASA grants NNX10AQ47G, NNX08AO48G, and NNG06GI95G. The computations were performed on NASA's Columbia supercomputer and on Kraken (a Cray XT5) at the National Institute for Computational Sciences. UCLA-IGPP publication 6479.

[34] Masaki Fujimoto thanks Elizaveta Antonova and another reviewer for their assistance in evaluating this paper.

References

Alexandrova, O., V. Carbone, P. Veltri, and L. Sorriso-Valvo (2008), Small-scale energy cascade of the solar wind turbulence, *Astrophys. J.*, *674*, 1153–1157, doi:10.1086/524056.

Alexandrova, O., J. Saur, C. Lacombe, A. Mangeney, J. Mitchell, S. J. Schwartz, and P. Robert (2009), Universality of solar-wind turbulent spectrum from MHD to electron scales, *Phys. Rev. Lett.*, *103*, 165003, doi:10.1103/PhysRevLett.103.165003.

Angelopoulos, V., T. Mukai, and S. Kokubun (1999), Evidence of intermittency in Earth's plasma sheet and implications for self-organized criticality, *Phys. Plasmas*, *6*, 4161–4168, doi:10.1063/1.873681.

Anselmet, F., Y. Gagne, E. J. Hopfinger, and R. A. Antonia (1984), Higher-order velocity structure functions in turbulent shear flows, *J. Fluid Mech.*, *140*, 63–89, doi:10.1017/S0022112084000513.

Antonova, E. E. (2000), Large scale magnetospheric turbulence and the topology of magnetospheric currents, *Adv. Space Res.*, *25*, 1567–1570, doi:10.1016/S0273-1177(99)00669-9.

Antonova, E. E., and I. L. Ovchinnikov (1999), Magnetostatically equilibrated plasma sheet with developed medium-scale turbulence: Structure and implications for substorm dynamics, *J. Geophys. Res.*, *104*(A8), 17,289–17,297, doi:10.1029/1999JA900141.

Ashour-Abdalla, M., M. El-Alaoui, V. Peroomian, R. J. Walker, L. M. Zelenyi, L. A. Frank, and W. R. Paterson (1999), Localized reconnection and substorm onset on Dec. 22, 1996, *Geophys. Res. Lett.*, *26*(23), 3545–3548, doi:10.1029/1999GL003630.

Ashour-Abdalla, M., M. El-Alaoui, F. V. Coroniti, R. J. Walker, and V. Peroomian (2002), A new convection state at substorm onset: Results from an MHD study, *Geophys. Res. Lett.*, *29*(20), 1965, doi:10.1029/2002GL015787.

Ashour-Abdalla, M., J.-M. Bosqued, M. El-Alaoui, V. Peroomian, M. Zhou, R. Richard, R. Walker, A. Runov, and V. Angelopoulos (2009), A simulation study of particle energization observed by THEMIS spacecraft during a substorm, *J. Geophys. Res.*, *114*, A09204, doi:10.1029/2009JA014126.

Biskamp, D. (1993), *Nonlinear Magnetohydrodynamics*, *Cambridge Monogr. Plasma Phys.*, *1*, 396 pp., Cambridge Univ. Press, New York.

Borovsky, J. E. (2004), A model for the MHD turbulence in the Earth's plasma sheet: Building computer simulations, in *Multiscale Processes in the Earth's Magnetosphere: From Interball to Cluster*, vol. 178, edited by J.-A. Sauvaud and Z. Memecek, pp. 217–253, Kluwer Acad., Dordrecht, Neth.

Borovsky, J. E., and H. O. Funsten (2003), The MHD turbulence in the Earth's plasma sheet: Dynamics, dissipation, and driving, *J. Geophys. Res.*, *108*(A7), 1284, doi:10.1029/2002JA009625.

Borovsky, J. E., R. C. Elphic, H. O. Funsten, and M. F. Thomsen (1997), The Earth's plasma sheet as a laboratory for turbulence in high-beta MHD, *J. Plasma Phys.*, *57*, 1–34, doi:10.1017/S0022377896005259.

Borovsky, J. E., M. F. Thomsen, and R. C. Elphic (1998), The driving of the plasma sheet by the solar wind, *J. Geophys. Res.*, *103*(A8), 17,617–17,639, doi:10.1029/97JA02986.

Bruno, R., and V. Carbone (2005), The solar wind as a turbulence laboratory, *Living Rev. Sol. Phys.*, *2*, lrsp-2005-4.

Castaing, B., Y. Gagne, and E. J. Hopfinger (1990), Velocity probability distribution functions of high Reynolds number turbulence, *Physica D*, *46*, 177–200, doi:10.1016/0167-2789(90)90035-N.

Chang, T. (1999), Self-organized criticality, multi-fractal spectra, sporadic localized reconnections and intermittent turbulence in the magnetotail, *Phys. Plasmas*, *6*, 4137–4145, doi:10.1063/1.873678.

Chen, S. Y., and R. H. Kraichnan (1989), Sweeping decorrelation in isotropic turbulence, *Phys. Fluids A*, *1*, 2019–2024, doi:10.1063/1.857475.

Claudepierre, S. G., S. R. Elkington, and M. Wiltberger (2008), Solar wind driving of magnetospheric ULF waves: Pulsations driven by velocity shear at the magnetopause, *J. Geophys. Res.*, *113*, A05218, doi:10.1029/2007JA012890.

Coleman, P. J. (1968), Turbulence, viscosity, and dissipation in the solar wind plasma, *Astrophys. J.*, *153*, 371, doi:10.1086/149674.

Collado-Vega, Y. M., R. L. Kessel, X. Shao, and R. A. Boller (2007), MHD flow visualization of magnetopause boundary region vortices observed during high-speed streams, *J. Geophys. Res.*, *112*, A06213, doi:10.1029/2006JA012104.

Consolini, G., and P. D. Michelis (1998), Non-Gaussian distribution function of AE-index fluctuations: Evidence for time intermittency, *Geophys. Res. Lett.*, *25*(21), 4087, doi:10.1029/1998GL900073.

Consolini, G., M. F. Marcucci, and M. Candidi (1996), Multifractal structures of auroral electrojet index data, *Phys. Rev. Lett.*, *76*, 4082–4085, doi:10.1103/PhysRevLett.76.4082.

El-Alaoui, M. (2001), Current disruption during November 24, 1996, substorm, *J. Geophys. Res.*, *106*(A4), 6229–6245, doi:10.1029/1999JA000260.

El-Alaoui, M., R. L. Richard, M. Ashour-Abdalla, and M. W. Chen (2004), Low Mach number bow shock locations during a magnetic cloud event: Observations and magnetohydrodynamic simulations, *Geophys. Res. Lett.*, *31*, L03813, doi:10.1029/2003GL018788.

El-Alaoui, M., M. Ashour-Abdalla, J. M. Bosqued, and R. L. Richard (2008), Understanding magnetotail current sheet meso-scale structures using MHD simulations, *Adv. Space Res.*, *41*(10), 1630–1642, doi:10.1016/j.asr.2007.05.061.

El-Alaoui, M., M. Ashour-Abdalla, R. J. Walker, V. Peroomian, R. L. Richard, V. Angelopoulos, and A. Runov (2009), Substorm evolution as revealed by THEMIS satellites and a global MHD simulation, *J. Geophys. Res.*, *114*, A08221, doi:10.1029/2009JA014133.

Fairfield, D., A. Otto, T. Mukai, S. Kokubun, R. Lepping, J. Steinberg, A. Lazarus, and T. Yamamoto (2000), Geotail observations of the Kelvin-Helmholtz instability at the equatorial magnetotail boundary for parallel northward fields, *J. Geophys. Res.*, *105*(A9), 21,159–21,173, doi:10.1029/1999JA000316.

Fairfield, D. H., M. M. Kuznetsova, T. Mukai, T. Nagai, T. I. Gombosi, and A. J. Ridley (2007), Waves on the dusk flank boundary layer during very northward interplanetary magnetic field conditions: Observations and simulation, *J. Geophys. Res.*, *112*, A08206, doi:10.1029/2006JA012052.

Frank, L., et al. (1995), Observations of plasmas and magnetic fields in Earth's distant magnetotail: Comparison with a Global MHD Model, *J. Geophys. Res.*, *100*(A10), 19,177–19,190, doi:10.1029/95JA00571.

Goldstein, M. L., and D. A. Roberts (1999), Magnetohydrodynamic turbulence in the solar wind, *Phys. Plasmas*, *6*, 4154–4159, doi:10.1063/1.873680.

Goldstein, M. L., D. A. Roberts, A. E. Deane, S. Ghosh, and H. K. Wong (1999), Numerical simulation of Alfvénic turbulence in the solar wind, *J. Geophys. Res.*, *104*(A7), 14,437–14,451, doi:10.1029/1998JA900128.

Grant, H. L., R. W. Stewart, and A. Moilliet (1962), Turbulence spectra from a tidal channel, *J. Fluid Mech.*, *12*(2), 241–268.

Guild, T. B., H. E. Spence, E. L. Kepko, V. Merkin, J. G. Lyon, M. Wiltberger, and C. C. Goodrich (2008), Geotail and LFM comparisons of plasma sheet climatology: 2. Flow variability, *J. Geophys. Res.*, *113*, A04217, doi:10.1029/2007JA012613.

Hasegawa, H., M. Fujimoto, T.-D. Phan, H. Reme, A. Balogh, M. W. Dunlop, C. Hashimoto, and R. TanDokoro (2004), Transport of solar wind into Earth's magnetosphere through rolled-up Kelvin-Helmholtz vortices, *Nature*, *430*, 755–758, doi:10.1038/nature02799.

Klimas, A. J., J. A. Valdivia, D. Vassiliadis, D. N. Baker, M. Hesse, and J. Takalo (2000), Self-organized criticality in the storm phenomenon and its relation to localized reconnection in the magnetospheric plasma sheet, *J. Geophys. Res.*, *105*(A8), 18,765–18,780, doi:10.1029/1999JA000319.

Kolmogorov, A. N. (1941), The local structure of turbulence in incompressible viscous fluid for very large Reynolds numbers, *C. R. Acad. Sci. URSS*, *30*, 301–321.

Kraichnan, R. H. (1965), Inertial range of hydromagnetic turbulence, *Phys. Fluids*, *8*, 1385–1387, doi:10.1063/1.1761412.

Leamon, R. J., C. W. Smith, N. F. Ness, and H. K. Wong (1999), Dissipation range dynamics: Kinetic Alfvén waves and the importance of β_e, *J. Geophys. Res.*, *104*(A10), 22,331–22,344, doi:10.1029/1999JA900158.

Lui, A. T. Y. (2001), Multifractal and intermittent nature of substormassociated magnetic turbulence in the magnetotail, *J. Atmos. Sol. Terr. Phys.*, *63*, 1379–1385, doi:10.1016/S1364-6826(00)00239-X.

Lui, A. T. Y. (2002), Multiscale phenomena in the near-Earth magnetosphere, *J. Atmos. Sol. Terr. Phys.*, *64*, 125–143, doi:10.1016/S1364-6826(01)00079-7.

Matthaeus, W. H., and M. L. Goldstein (1982a), Stationarity of magnetohydrodynamic fluctuations in the solar wind, *J. Geophys. Res.*, *87*(A12), 10,347–10,354, doi:10.1029/JA087iA12p10347.

Matthaeus, W. H., and M. L. Goldstein (1982b), Measurement of the rugged invariants of magnetohydrodynamic turbulence in the solar wind, *J. Geophys. Res.*, *87*(A8), 6011–6028, doi:10.1029/JA087iA08p06011.

Matthaeus, W. H., and S. L. Lamkin (1986), Turbulent magnetic reconnection, *Phys. Fluids*, *29*, 2513–2535, doi:10.1063/1.866004.

Matthaeus, W. H., M. L. Goldstein, and C. Smith (1982), Evaluation of magnetic helicity in homogeneous turbulence, *Phys. Rev. Lett.*, *48*, 1256–1259, doi:10.1103/PhysRevLett.48.1256.

Matthaeus, W. H., J. M. Weygand, P. Chuychai, S. Dasso, C. W. Smith, and M. G. Kivelson (2008), Interplanetary magnetic Taylor microscale and implications for plasma dissipation, *Astrophys. J.*, *678*, L141–L144, doi:10.1086/588525.

Matthieu, J., and J. Scott (2000), *An Introduction to Turbulent Flow*, Cambridge Univ. Press, New York.

Nykyri, K., and A. Otto (2001), Plasma transport at the magnetospheric boundary due to reconnection in Kelvin-Helmholtz vortices, *Geophys. Res. Lett.*, *28*(18), 3565–3568, doi:10.1029/2001GL013239.

Nykyri, K., B. Grison, P. J. Cargill, B. Lavraud, E. Lucek, I. Dandouras, A. Balogh, N. Cornilleau-Wehrlin, and H. Rème (2006a), Origin of the turbulent spectra in the high-altitude cusp: Cluster spacecraft observations, *Ann. Geophys.*, *24*, 1057–1075, Available at www.ann-geophys.net/24/1057/2006/, doi:10.5194/angeo-24-1057-2006.

Nykyri, K., A. Otto, B. Lavraud, C. Mouikis, L. M. Kistler, A. Balogh, and H. Rème (2006b), Cluster observations of reconnection due to the Kelvin-Helmholtz instability at the dawnside magnetospheric flank, *Ann. Geophys.*, *24*, 2619–2643, doi:10.5194/angeo-24-2619-2006.

Perri, S., and A. Balogh (2010), Stationarity in solar wind flows, *Astrophys. J.*, *714*, 937–943, doi:10.1088/0004-637X/714/1/937.

Pope, S. B. (2000), *Turbulent Flows*, Cambridge Univ. Press, New York.

Raeder, J., R. J. Walker, and M. Ashour-Abdalla (1995), The structure of the distant geomagnetic tail during long periods of northward IMF, *Geophys. Res. Lett.*, *22*(4), 349–352, doi:10.1029/94GL03380.

Raeder, J., J. Berchem, and M. Ashour-Abdalla (1996), The importance of small scale processes in global MHD simulations: Some numerical experiments, in *The Physics of Space Plasmas*, vol. 14, edited by T. Chang and J. R. Jasperse, p. 403, Mass. Inst. of Technol. Cent. for Theor. Geo/Cosmo Plasma Phys., Cambridge, Mass.

Raeder, J., J. Berchem, and M. Ashour-Abdalla (1998), The Geospace Environment Modeling Grand Challenge: Results from a global geospace circulation model, *J. Geophys. Res.*, *103*(A7), 14,787–14,797, doi:10.1029/98JA00014.

Raeder, J., R. L. McPherron, L. A. Frank, S. Kokubun, G. Lu, T. Mukai, W. R. Paterson, J. B. Sigwarth, H. J. Singer, and J. A. Slavin (2001), Global simulation of the Geospace Environment Modeling substorm challenge event, *J. Geophys. Res.*, *106*(A1), 381–395, doi:10.1029/2000JA000605.

Reiff, P. H., R. W. Spiro, and T. W. Hill (1981), Dependence of polar cap potential drop of interplanetary parameters, *J. Geophys. Res.*, *86*(A9), 7639–7648, doi:10.1029/JA086iA09p07639.

Roberts, D., L. Klein, M. Goldstein, and W. Matthaeus (1987a), The nature and evolution of magnetohydrodynamic fluctuations in the solar wind: Voyager observations, *J. Geophys. Res.*, *92*(A10), 11,021–11,040, doi:10.1029/JA092iA10p11021.

Roberts, D., M. Goldstein, L. Klein, and W. Matthaeus (1987b), Origin and evolution of fluctuations in the solar wind: Helios observations and Helio-Voyager comparisons, *J. Geophys. Res.*, *92*(A11), 12,023–12,035, doi:10.1029/JA092iA11p12023.

Sahraoui, F., M. L. Goldstein, P. Robert, and Y. V. Khotyaintsev (2009), Evidence of a cascade and dissipation of solar-wind turbulence at the electron gyroscale, *Phys. Rev. Lett.*, *102*, 231102–231106, doi:10.1103/PhysRevLett.102.231102.

Sato, T., and T. Hayashi (1979), Externally driven magnetic reconnection and a powerful magnetic energy converter, *Phys. Fluids*, *22*, 1189–1203, doi:10.1063/1.862721.

Slinker, S. P., J. A. Fedder, D. G. Sibeck, J. G. Lyon, L. A. Frank, and T. Mukai (2003), Simulation of magnetopause oscillations observed January 9, 1996, *Geophys. Res. Lett.*, *30*(11), 1569, doi:10.1029/2003GL017063.

Sonnerup, B. U. Ö., K. D. Siebert, W. W. White, D. R. Weimer, N. C. Maynard, J. A. Schoendorf, G. R. Wilson, G. L. Siscoe, and G. M. Erickson (2001), Simulations of the magnetosphere for zero interplanetary magnetic field: The ground state, *J. Geophys. Res.*, *106*(A12), 29,419–29,434, doi:10.1029/2001JA000124.

Sorriso-Valvo, L., V. Carbone, P. Veltri, G. Consolini, and R. Bruno (1999), Intermittency in the solar wind turbulence through probability distribution functions of fluctuations, *Geophys. Res. Lett.*, *26*(13), 1801–1804, doi:10.1029/1999GL900270.

Taylor, G. I. (1938), The spectrum of turbulence, *Proc. R. Soc. London, Ser. A*, *164*, 476–490, doi:10.1098/rspa.1938.0032.

Tennekes, H. (1975), Eulerian and Lagrangian time microscales in isotropic turbulence, *J. Fluid Mech.*, *67*, 561–605, doi:10.1017/S0022112075000468.

Vörös, Z., W. Baumjohann, R. Nakamura, A. Runov, M. Volwerk, H. Schwarzl, A. Balogh, and H. Rème (2005), Dissipation scales in the Earth's plasma sheet estimated from Cluster measurements, *Nonlinear Processes Geophys.*, *12*, 725–732, doi:10.5194/npg-12-725-2005.

Vörös, Z., W. Baumjohann, R. Nakamura, M. Volwerk, and A. Runov (2006), Bursty bulk flow driven turbulence in the Earth's plasma sheet, *Ann. Geophys.*, *21*, 1955–1964.

Walker, R. J., T. Ogino, and M. Ashour-Abdalla (1998), The response of the magnetosphere to a solar wind density pulse, in *Substorms-4: International Conference on Substorms-4, Lake Hamana, Japan, March 9–13, 1998*, edited by S. Kokubun and Y. Kamide, p. 527, Terra Sci., Tokyo.

Walker, R. J., M. Ashour-Abdalla, M. El-Alaoui, and F. V. Coroniti (2006), Magnetospheric convection during prolonged intervals with southward interplanetary magnetic field, *J. Geophys. Res.*, *111*, A10219, doi:10.1029/2005JA011541.

Weygand, J. M., et al. (2005), Plasma sheet turbulence observed by Cluster II, *J. Geophys. Res.*, *110*, A01205, doi:10.1029/2004JA010581.

Weygand, J. M., M. G. Kivelson, K. K. Khurana, H. K. Scwarzl, R. J. Walker, A. Balogh, L. M. Kistler, and M. L. Goldstein (2006), Non self-similar scaling of plasma sheet and solar wind probability distribution functions of magnetic field fluctuations, *J. Geophys. Res.*, *111*, A11209, doi:10.1029/2006JA011820.

Weygand, J. M., W. H. Matthaeus, S. Dasso, M. G. Kivelson, and R. J. Walker (2007), Taylor scale and effective magnetic Reynolds number determination from plasma sheet and solar wind magnetic field measurements, *J. Geophys. Res.*, *112*, A10201, doi:10.1029/2007JA012486.

White, W. W., J. A. Shoendorf, K. D. Siebert, N. C. Maynard, D. R. Weimer, G. L. Wilson, B. U. O. Sonnerup, G. L. Siscoe, and G. M. Erickson (2001), MHD simulation of magnetospheric transport at the mesoscale, in *Space Weather*, *Geophys. Monogr. Ser.*, vol. 125, edited by P. Song, H. Singer, and G. Siscoe, pp. 229–240, AGU, Washington, D. C.

M. Ashour-Abdalla, M. El-Alaoui, R. L. Richard, R. J. Walker, and J. M. Weygand, Institute of Geophysics and Planetary Physics, University of California, Los Angeles, 405 Hilgard Ave., Los Angeles, CA 90095-1567, USA. (mostafa@igpp.ucla.edu)

M. L. Goldstein, Laboratory for Geospace Science, NASA Goddard Space Flight Center, Code 673, Greenbelt, MD 20771, USA.